



## Light recycling in LED-pumped Ce:YAG luminescent concentrators

Maxime Nourry-Martin, P. Pichon, Frederic Druon, Stephane Darbon,  
François Balembois, Patrick Georges

### ► To cite this version:

Maxime Nourry-Martin, P. Pichon, Frederic Druon, Stephane Darbon, François Balembois, et al..  
Light recycling in LED-pumped Ce:YAG luminescent concentrators. *Optics Express*, 2021, 29 (16),  
pp.25302. 10.1364/oe.433063 . hal-03298463

**HAL Id: hal-03298463**


**<https://hal.science/hal-03298463>**

Submitted on 23 Jul 2021

**HAL** is a multi-disciplinary open access archive for the deposit and dissemination of scientific research documents, whether they are published or not. The documents may come from teaching and research institutions in France or abroad, or from public or private research centers.

L'archive ouverte pluridisciplinaire **HAL**, est destinée au dépôt et à la diffusion de documents scientifiques de niveau recherche, publiés ou non, émanant des établissements d'enseignement et de recherche français ou étrangers, des laboratoires publics ou privés.

# Light recycling in LED-pumped Ce:YAG luminescent concentrators

MAXIME NOURRY-MARTIN,<sup>1,2,\*</sup> PIERRE PICHON,<sup>1</sup> FREDERIC DRUON,<sup>1</sup>  STEPHANE DARBON,<sup>2</sup> FRANÇOIS BALEMBOIS,<sup>1</sup> AND PATRICK GEORGES<sup>1</sup>

<sup>1</sup>Université Paris-Saclay, Institut d'Optique Graduate School, CNRS, Laboratoire Charles Fabry, 91127, Palaiseau, France

<sup>2</sup>CEA, DAM, DIF, F-91297 Arpajon, France

\*maxime.nourry-martin@institutoptique.fr

**Abstract:** We report the development of a high-brightness, high-power Ce:YAG luminescent concentrator pumped by 2240 blue LEDs in quasi-continuous wave operation (10  $\mu$ s, 10 Hz). Using light confinement and recycling in the three space dimensions, the parallelepiped (1mm $\times$ 14mm $\times$ 200mm) Ce:YAG emits a power of 145 W from a square output surface (1 $\times$ 1mm<sup>2</sup>) corresponding to a brightness of 4.6 kW/cm<sup>2</sup>/sr. This broadband yellow source has a unique combination of luminous flux (7.6 10<sup>4</sup> lm) and brightness (2.4 10<sup>4</sup> cd/mm<sup>2</sup>) and overcomes many other visible incoherent sources by one order of magnitude. This paper also proposes a deep understanding of the performance drop compared to a linear behavior when the pump power increases. Despite excited state absorption was unexpected for this low doped Ce:YAG pumped at a low irradiance level, we demonstrated that it affects the performance by tripling the losses in the concentrator. This effect is particularly important for small output surfaces corresponding to strong light recycling in the concentrator and to average travel distances inside the medium reaching meters.

© 2021 Optical Society of America under the terms of the [OSA Open Access Publishing Agreement](#)

## 1. Introduction

InGaN blue light-emitting diodes (LED) became a mature technology not only at the center of the domestic and automotive lighting market but also for other applications in the field of machine vision, medical lighting, digital projection, display, and metrology. LEDs can be characterized by their power and by their brightness corresponding to the power divided by the emitting area and emitting solid angle (expressed in W/cm<sup>2</sup>/sr in radiometric units). Both parameters have improved significantly since the design of blue light-emitting diodes in 1994 by Nakamura *et al* [1]. Starting from a brightness estimated to 0.05 W/cm<sup>2</sup>/sr [1]. This evolved quickly to 0.3 W/cm<sup>2</sup>/sr in 1999 [2], 10 W/cm<sup>2</sup>/sr in 2007 (K2 line by Lumiled), 30 W/cm<sup>2</sup>/sr in 2015 (Luxeon Z line by Lumiled) and 80 W/cm<sup>2</sup>/sr in 2020 (Rubix line by Lumiled). With a typical power at the watt level on a 1 mm<sup>2</sup> emitting area, LED performance face fundamental limitation caused by the “efficiency drop” at high injected current [3]. Fortunately, LED packaging has considerably progressed. With high density compact chip-scale package, LEDs can be arranged as “pixels” in large arrays for power scaling. However, the brightness of the array can only be degraded compared to a single LED because of the limited filling factor of LEDs emitting surfaces on the array. Despite all LED’s advantages (ruggedness, long lifetime, efficiency, and low price), many applications in illumination like RGB projection, 3D inspection, or treatment in dermatology, require a combination of power and brightness that cannot be addressed by LED even arranged in arrays.

The brightness conservation theorem states that an emitting surface cannot be reimaged to a higher brightness than the source itself using a passive ray-optical system [4]. Hence, to exceed LED’s performance, alternative light sources must be imagined out of the scope of this theorem.

An idea coming in the late 1990s is based on wavelength conversion, associating InGaN blue LEDs, as pump sources, with a cerium-doped yttrium aluminum garnet (Ce:YAG) phosphor to generate white light [5,6]. Indeed, Ce:YAG is a highly chemical stable phosphor [7] showing excellent spectroscopic properties with a emission peaking at the maximum human eye sensitivity. Ce:YAG absorption is centered at 460 nm and its emission spectrum peaks at 550 nm and with a FWHM bandwidth of 100 nm. In the mid-2010s, to increase the brightness, research groups proposed to replace blue LEDs by high brightness laser diodes. Laser activated remote phosphor [8] create small fluorescent point sources with highly doped Ce:YAG small plate [9–10]. The brightness reaches  $560 \text{ W/cm}^2/\text{sr}$  ( $3000 \text{ cd/mm}^2$ ) but with a power limited to the watt level (850 lumens) [9] by the power of laser diodes and by thermal management in Ce:YAG. In addition, laser diodes are less robust than LED and their typical lifetime is approximately 10 000 hours whereas LEDs only lose 20% of their optical power after 50 000 hours of use. The next step for brightness and power increases was achieved by pumping large plates of Ce:YAG with blue LED arrays. The parallelepiped, polished on all faces, acts as a waveguide for the light emitted by  $\text{Ce}^{3+}$  ions. The largest faces are used to pump the crystal and one of the smallest lateral faces is used as output face. This concept has been used for many years in solar luminescent concentrators [11] offering a brightness enhancement with respect to the sun thanks to the absorption/emission process combined with the geometry of the parallelepiped. Pumped by LED, this setup is referred as “LED-pumped luminescent concentrator” (LED-LC). Such device can deliver peak powers reaching  $1\,200 \text{ W/cm}^2/\text{sr}$  in quasi-continuous wave operation [12]. In continuous wave operation the brightness reaches the  $100 \text{ W/cm}^2/\text{sr}$  range ( $230 \text{ W/cm}^2/\text{sr}$  [13] and  $110 \text{ W/cm}^2/\text{sr}$  [14]). With this unique combination of power and brightness for incoherent sources, LED-LC have been successfully used for solid-state laser pumping [12, 15, 16] medical imaging [13] and digital projection [14].

Recently, it has been proposed to confine the light inside a LC in the three dimensions of space via total internal reflections (TIR) on the 4 faces parallel to the output axis and by using mirrors on the faces perpendicular to the output axis [17]. This setup, referred as 3D luminescent concentrators (3D-LC), has the potential to increase the brightness of the LC by one order of magnitude. The first proof of concept was performed at low pump power: a 1 W blue laser diode was shaped in a large and homogeneous beam corresponding to the size of the largest face of a Ce:YAG luminescent concentrator.

In this paper, we propose a step further by pumping a 3D Ce:YAG luminescent concentrator with high power blue LED arrays. Experiment and performance are described in a first part. Limitations of performance, attributed to excited state absorption (ESA) are experimentally investigated and analytically described in a second part.

## 2. Experimental setup and performance

### 2.1. Experimental setup

Blue LEDs with an emission spectrum centered on 450 nm and a spectral full width at half maximum of 20 nm are used in this experiment (Luxeon Z royal blue from Lumiled whose spectrum can be found in [12]). This chip-scale package LED has been chosen for its compacity ( $1 \times 1 \text{ mm}^2$  emitting area for a  $1.7 \times 1.3 \text{ mm}^2$  package). The quasi-continuous wave operation allows to overdrive LED above their nominal driving current (1 A). When the LED is activated during 10  $\mu\text{s}$  at 10 Hz, LED's driven current can be increased up to 7 A resulting in an optical peak power of 4.2 W (peak brightness of  $133 \text{ W/cm}^2/\text{sr}$ ). In this quasi-continuous wave operation, the corresponding forward voltage is 5.2 V and the electro/optic efficiency of the LED is 12%. The compactness of the LED package allows to build high-density LED arrays brazed on a water-cooled aluminum printed circuit board (PCB). Each PCB is composed of 280 LEDs divided in 35 lines of 8 LEDs. 8 PCB (gathered by 4) are positioned side by side resulting in two

200×14 mm<sup>2</sup> LED arrays of 1120 elements. This corresponds to a filling factor (portion of emitting surface on the array) of 42%.

The luminescent concentrator is composed of two  $l=100$  mm,  $w=14$  mm and  $t=1$  mm Ce:YAG slabs bonded with a UV-curing optical adhesive resulting in a total length of 200 mm (Fig. 1). All the sides of the LC are optically polished to scratch/dig 60/40. The  $\text{Ce}^{3+}$  concentration is  $9.9 \cdot 10^{18} \text{ cm}^{-3}$  corresponding to an average absorption coefficient of  $18 \text{ cm}^{-1}$  over the LED emission spectrum. The PCBs are pump close to the large faces of the concentrator ( $< 1$  mm). Taking the filling factor of the PCBs (42%) in account, we estimate the average pump intensity on the Ce:YAG large faces at  $1.8 \text{ W/mm}^2$ .

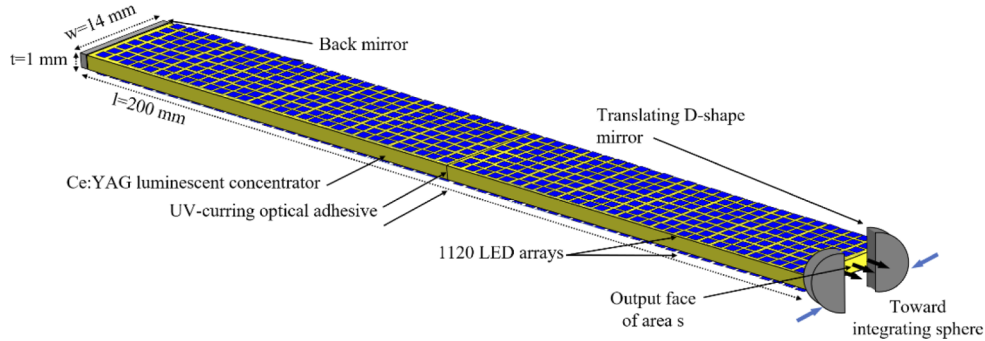


**Fig. 1.** Schematic representation of the blue LED-pumped Ce:YAG luminescent concentrator used in this experiment.

A HR back mirror is positioned on one of the  $w \times t$  face which corresponds to the facet opposite to the output. To complete the light recycling process in the third dimension, two D-shaped mirrors are put close to the output face reducing the output surface (area denoted  $s$ ). The two D-shaped mirrors are fixed on a digital sliding caliper which enable to measure and to control the length of the aperture. The ratio  $r = wt/s$  ( $r \geq 1$ ) can be varied by a translation of the mirrors in a direction perpendicular to the output direction. All the mirrors used in this experiment have a reflectivity of 99.4% on the emission range of Ce:YAG (E02 coating from Thorlabs).

## 2.2. Performance of the LED-pumped 3D luminescent concentrator and evidence of ESA limitation

The LEDs operate in quasi-continuous wave operation ( $10 \mu\text{s}$  at  $10 \text{ Hz}$ ). An integrating sphere coupled to a spectrometer (LCS-100 from Labsphere) is placed directly in front of the  $w \times t$  output face to measure the average power emitted by this surface. To evaluate precisely the emitted peak power over the  $10 \mu\text{s}$  pumping window, the duration of the emitted pulses is recorded by a photodiode put on a leakage of the concentrator.

The evolution of the power emitted by the  $w \times t$  face of the LC as a function of the peak power emitted by the LED array is shown in Fig. 2. The LED are driven with a current from 1 A to 7 A with a step of 1 A. The corresponding pump peak power ranges from 2.9 kW to 9.4 kW. For  $r=1$  (output face without mirrors), the emitted peak power reaches 724 W and the brightness  $1.6 \text{ kW/cm}^2/\text{sr}$ . For an output surface close of  $1 \text{ mm}^2$  ( $r=14$ ) the peak power and brightness of the LC are respectively 145 W and  $4.6 \text{ kW/cm}^2/\text{sr}$ . The smallest aperture achieved is  $0.2 \text{ mm}^2$  ( $r=70$ ) for which a power of 33 W and a brightness of  $5.3 \text{ kW/cm}^2/\text{sr}$  are reached.

Compared to the expected proportional behavior, we observe a discrepancy of the output power, more important for higher  $r$  values (Fig. 2(b)). For  $r=1$ , the power drops by 14% at maximum pump power compared to a linear behavior. For an output surface of  $1 \text{ mm}^2$  ( $r=14$ ),

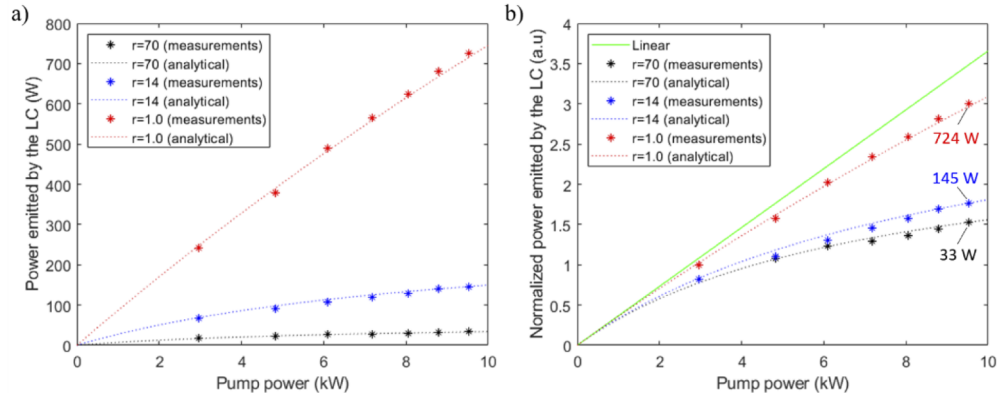


**Fig. 2.** (a) Power emitted the LC versus the pump power for  $r=1$ ,  $r=14$  and  $r=70$  ( $r = \text{wt/s}$ ). In (b) the  $r=1$ ,  $r=14$  and  $r=70$  curves are normalized in order to have the same tangent to the origin which describes the linear behavior without ESA.

the power drops by 50% at maximum pump power. Figure 2 indicates that a pump-intensity-dependent phenomenon is involved. As the repetition rate (10 Hz) and the activation duration (10  $\mu\text{s}$ ) are extremely low, this drop cannot be attributed to thermal effects. Previous works related to the spectroscopy of Ce:YAG under high pump intensities [8] suggest that two main loss mechanisms can occur: energy transfer upconversion (ETU) to the conduction band and excited-state absorption (ESA). ETU corresponds to energy transfer involving two  $\text{Ce}^{3+}$  ions in the excited state situated in nearby lattices. ETU depends quadratically on the concentration. It is classically observed in Ce:YAG for  $\text{Ce}^{3+}$  doping concentration higher than 1% and nearly not detectable for a concentration around 0.2% [8]. As our concentration is estimated to 0.11%, this effect can be neglected. The effect of ESA in Ce:YAG has been studied in previous works [18–21].

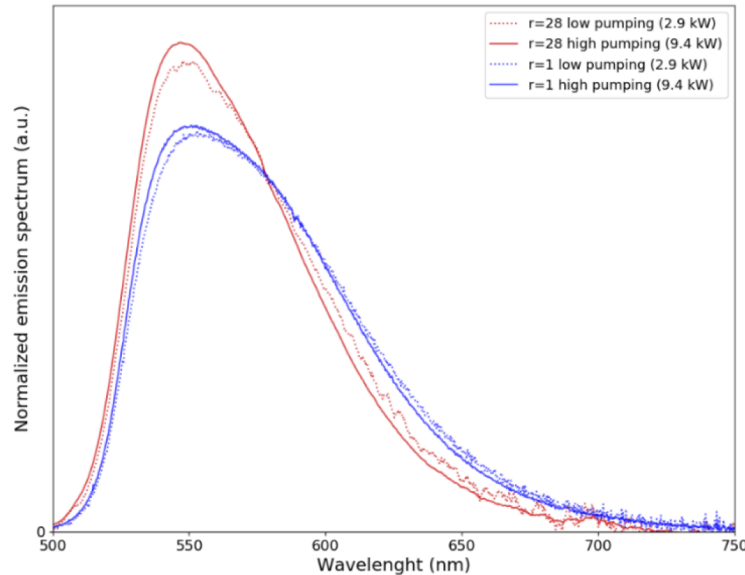


**Fig. 3.** Normalized spectra (lineshape functions) emitted by the LC at two pump powers 2.9 kW and 9.4 kW for  $r=1$  (a) and  $r=28$  (b).

The amplitude of ESA is wavelength dependent [18]: being much higher above 600 nm than below. Hence, the distortion of the emitted spectrum for different pump powers and/or different values of  $r$  can be a signature of the presence of ESA. To analyze this effect, we compared the emitted spectra for two power levels 2.9 kW (1A driving current) and 9.4 kW (7A driving current) corresponding to the lowest and highest pumping level possible, taking the LED driver in account. The spectra are also recorded for two values of  $r$  ( $r=1$  and  $r=28$ ). For the sake of comparison, the spectra are normalized by their area, like any lineshape function (Fig. 3). One can observe a spectral narrowing on the red part for the highest pumping level compared to the lowest pumping level. This effect could be related to the presence of ESA, the population of the excited state being an increasing function of the pump power. The spectral narrowing is more visible for  $r=28$  than for  $r=1$ . This can be attributed to a higher travel distance for  $r=28$  than for  $r=1$  for the rays before finding the output.

Table 1 gives an overview of the LED array and luminescent concentrator performance. Despite the limitations observed, we obtained a record brightness above  $5 \text{ kW/cm}^2/\text{sr}$  in quasi-continuous wave operation overcoming the LED brightness by a factor 40.

**Table 1. Characteristics of the light sources used or build in this article. All the sources are driven in the same quasi-continuous wave operation (10  $\mu\text{s}$ , 10 Hz). \*Luxeon Z royal blue by Lumiled.**

	Single InGaN LED*	Pump from the 2 LED array (2240 LED)	This work with LED-pumped 3D-LC		
			$r=1$	$r=14$	$r=70$
Peak power (W)	4.2	9048	723	145	33
Area ( $\text{mm}^2$ )	1	5600	14	1	0.2
Brightness ( $\text{W/cm}^2/\text{sr}$ )	133	53	1646	4634	5256
Efficiency (%)	12% (e/o)	12% (e/o)	7.6% (o/o)	1.5% (o/o)	0.35% (o/o)
$B/B_{LED}$	1	0.40	12	35	40

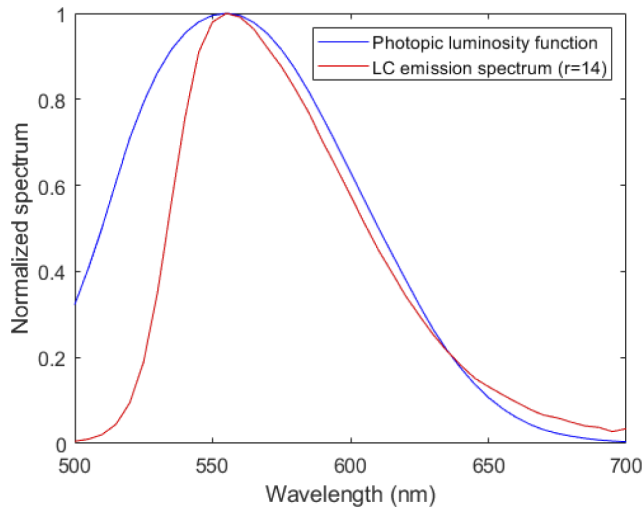


**Fig. 4.** Photopic luminosity function (eye's responsivity) and Ce:YAG luminescent concentrator emission spectrum ( $r=14$ ).



As the concentrator emits in the visible spectrum, it is interesting to estimate its power in lumens, taking the spectrum of the source and the response of the eye versus the wavelength (Fig. 4). Calculations are done for the  $r=14$  performance, presenting the best compromise between power and brightness. The source presents a luminous efficacy of 525 lm/W. It emits a power of  $7.6 \cdot 10^4$  lm with a brightness of  $2.4 \cdot 10^4$  cd/mm<sup>2</sup>. Compared to laser activated remote phosphors using Ce:YAG, this is one order of magnitude higher for the brightness and nearly two order of magnitude higher for the power.

### 3. Role of ESA in a 3D LED-pumped Ce:YAG luminescent concentrator

Excited State Absorption (ESA) has two main consequences on the Ce:YAG LC. It reduces the population density of the excited state ( $n_2$ ) and it induces additional propagation losses ( $\alpha_{ESA} = \sigma_{ESA} n_2$  with  $\sigma_{ESA}$  the ESA cross section). The aim of this section is to describe analytically how ESA affects the output power emitted by the LED-LC and to compare this model with the experimental results of the output powers.

#### 3.1. ESA and trapped rays

In order to simplify the approach, it is assumed that the LC emits at a single wavelength (the mean wavelength of the Ce:YAG LC emission spectrum is 580 nm) and we consider a mean value of the ESA cross section over the Ce:YAG emission spectrum. In a same way, reabsorption effects are integrated over all the emission spectrum and taken in account as part of the loss coefficient. As developed in [18], the stimulated emission cross section is neglected with respect to the value of the ESA cross section. In the ESA process, an electron of the excited state of a  $Ce^{3+}$  ion is sent to the conduction band and then relaxes quickly either in traps, or in the excited state, or in the ground state. The recombination branching ratio (fraction of  $Ce^{3+}$  ion from the conduction band population that recombines non-radiatively into the excited state) is denoted  $f$  and estimated to be 0.5 following [8].

As the pump duration (10  $\mu$ s) is considerably longer than the  $Ce^{3+}$  emission lifetime (64 ns [19]), the calculation of the population density  $n_2$  can be carried out in the steady state. Assuming that the decay rate from the conduction band is much higher than the other rates,  $n_2$  can be written as :

$$n_2 = \frac{\sigma_p n_t I_p}{A + f \sigma_{ESA} I_e} \quad (1)$$

where,  $\sigma_p$  is the absorption cross section of Ce:YAG on the LED spectrum,  $n_t$  is the total population density,  $A$  is the radiative decay rate,  $I_p$  and  $I_e$  are respectively the photonic intensities at the pump and emitted wavelengths. For simplicity, we assume that  $I_p$  and  $I_e$  are homogeneous in all the LC volume, leading to a constant value for  $n_2$  in all the Ce:YAG. By averaging the pump intensity over all the concentrator,  $I_p$  can be written as :

$$I_p = \frac{2P_{Array} T_{Fresnel}}{lwt} \frac{\lambda_p}{hc} \frac{(1 - e^{-\alpha_p l})}{\alpha_p} \quad (2)$$

where  $P_{Array}$  is the pump power of one array (4 PCBs),  $\alpha_p$  is the absorption coefficient  $\alpha_p = \sigma_p n_t$ ,  $l, w, t$  are the spatial dimensions of the LC (see Fig. 1),  $h$  is the Planck constant,  $c$  is the speed of light in vacuum and  $\lambda_p$  is the mean wavelength of a pump photon,  $T_{Fresnel}$  is the Fresnel transmission at the Ce:YAG / air interface (detailed in Table 2).

In Eq. (1), one key point is the intensity inside the LC at the emitted wavelength  $I_e$ . Assuming that a total internal reflection is lossless,  $I_e$  is mostly due to indefinitely trapped rays with no possible escape of faces. They represent a proportion  $(3 \cos \theta_{TIR} - 2)$  of the total emitted power, corresponding to 51% in the case of Ce:YAG in air ( $\theta_{TIR}$  is defined in Table 2). At a given point inside the LC, trapped rays superimpose incoherently after many reflections. In other words,

**Table 2. Parameters used for the analytical description of the power emitted by the LC.**

Parameter description	Parameter	Comments
Length of the LC	$l=200$ mm	$\pm 0.1$ mm
Width of the LC	$w=14$ mm	$\pm 0.1$ mm
Thickness of the LC	$t=1$ mm	$\pm 0.1$ mm
Refractive index of the LC	$n_{LC}=1.83$	
Fresnel Transmission	$T_{Fresnel}=0.91$	Approximated by (without polarization dependence) $T_{Fresnel} = 1 - [(n_{LC} - 1)/(n_{LC} + 1)]^2$
Angle of TIR (Ce:YAG/air)	$\theta_{TIR}=33^\circ$	$\sin \theta_{TIR} = 1/n_{LC}$
Reflectivity of the back mirror	$R=99.4\%$	Averaged on the emission spectrum (E02 coating from Thorlabs)
Transmission of the UV optical adhesive	$T_{OA}=97.5\%$	Vitalit VBB-1 ( $n=1.5$ ) (fit parameter)
Trapped light losses between two reflections	$L=0.2\%$	Escape possibilities of the trapped light (fit parameter)
Ce <sup>3+</sup> doping concentration	$n_t = 9.9 \times 10^{18} \text{ cm}^{-3}$	Measured via the transmission of a 450 nm laser diode on through 1 mm of Ce:YAG
Power emitted by one of the LED array	$P_{Array}$	$P_{Array}=4704$ W when LED at maximum driving current of 7A
Mean pump wavelength	$\lambda_p=450$ nm	Mean wavelength of the LED
Mean emitted wavelength	$\lambda_e=580$ nm	Mean wavelength of the emitted spectrum
Average intensity at the pump wavelength	$I_p$	Eq.2 (reaches $140 \text{ W/cm}^2$ at maximum pump power)
Average intensity at the emitted wavelength	$I_e$	Eq.3 (reaches $54 \text{ kW/cm}^2$ at maximum pump power)
Radiative decay rate	$A=1.56 \times 10^7 \text{ s}^{-1}$	$A=1/\tau$ with $\tau=64$ ns [18]
Population density in the excited state	$n_2$	Eq.1
Absorption coefficient of the ESA	$\alpha_{ESA}$	$\alpha_{ESA}=\sigma_{ESA} n_2$
ESA absorption cross section	$\sigma_{ESA}=12 \cdot 10^{-18} \text{ cm}^2$	Same order of magnitude as in [16], here it considers the average ESA on the emission spectrum and ESA is higher for longer wavelengths based on [18].
Absorption coefficient other than ESA	$\alpha=1.9 \times 10^{-3} \text{ cm}^{-1}$	$\alpha=1.63 \times 10^{-22} \times n_t + 2.85 \times 10^{-4}$ evaluated at low pump intensity without impact of ESA.
Average absorption coefficient on the LED spectrum	$\alpha_p=18 \text{ cm}^{-1}$	Measured by the transmission of an LED through 1 mm of Ce:YAG
Recombination branching ratio	$f=0.5$	According to [8]



each time that a trapped ray is reflected, the reflection increases the intensity inside the LC. The distance between two reflections can be estimated assuming that reflections occur mostly between the two large faces. Observing that the main angular directions of trapped rays corresponds to an annulus between  $\theta_{TIR}$  and  $90^\circ - \theta_{TIR}$  (Fig. 5), the distance between two reflections is estimated to  $1.44t$  for Ce:YAG, by averaging all the possible distances between the two largest faces for trapped rays.

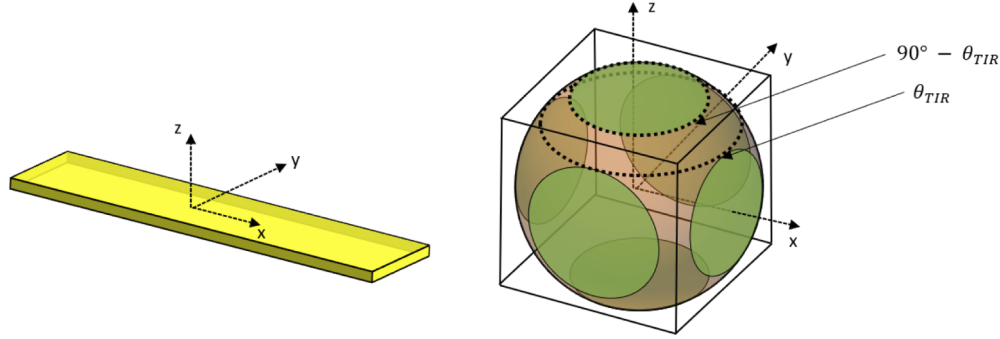


**Fig. 5.** Representation of the internal rays in a luminescent concentrator. The dotted cap shows the main location of trapped rays considered in the analytical model.

In practice the number of reflections is not infinite because of the propagation losses and because of LC surface imperfections (imperfect chamfers on the edges, diffusion or dusts on the surfaces and quality of the surfaces). Using the concept of light recycling,  $I_e$  can be estimated by the sum of the terms of a geometric series as follows (see [Supplement 1](#)):

$$I_e = (3 \cos \theta_{TIR} - 2) \frac{1.44tAn_2}{1 - (1 - L)e^{-1.44t(\alpha + \alpha_{ESA})}} \quad (3)$$

where  $\alpha$  is the propagation loss coefficient other than ESA and depends linearly on the  $\text{Ce}^{3+}$  concentration (see Table 2). The parameter  $L$  corresponds to the losses related to surface imperfections. It reduces the trapped intensity at each reflection. It is used as a fit parameter and estimated to be 0.2%.

### 3.2. Output power for a 2D-luminescent concentrator ( $r=1$ )

As a first step, we suppose that the output surface is the total  $w \times t$  face ( $r=1$ ). This configuration refers as LED-LC operating with a confinement in 2 dimensions. Considering ESA and based on [15], the power emitted by the LC on the  $w \times t$  face is:

$$P_{2D} = An_2 w t l \frac{hc}{\lambda_e} \frac{(\cos \theta_{TIR} - 1)}{2d_l(\alpha + \alpha_{ESA})} \frac{T_{Fresnel}(e^{-d_l(\alpha + \alpha_{ESA})} - 1)(1 + RT_{OA}^2 e^{-d_l(\alpha + \alpha_{ESA})})}{1 - e^{-2d_l(\alpha + \alpha_{ESA})}[RT_{OA}^2(1 - T_{Fresnel})]} \quad (4)$$

$d_l$  is the average distance in the escape cone of the output face, being defined by:

$$d_l = l \frac{-\ln(\cos \theta_{TIR})}{(1 - \cos \theta_{TIR})} \quad (5)$$

In Eq. (4)  $\lambda_e$  is the mean emitted wavelength,  $R$  is the reflectivity of the back mirror (Fig. 1) and  $T_{OA}$  is the transmission of the optical adhesive used to bond the two LC. All the parameters used are gathered in Table 2.

The ESA absorption cross section used in the analytical model is set to  $\sigma_{ESA} = 12 \cdot 10^{-18} \text{ cm}^2$  for an optimal fit of the measurements. There is a strong fluctuation on the values of  $\sigma_{ESA}$  in the

literature [8,19]. Our analytical model requires a mean value of  $\sigma_{ESA}$  weighted by the emission spectrum of Ce:YAG which is in the same order of magnitude than the values of the literature.

Equation (4) is used to plot the analytical red curves ( $r=1$ ) on Fig. 2 and fits the experimental observation. The analytical model shows that ESA gives a good description of the performance deviation compared to a linear evolution. The analytical model can help to estimate the two effects of ESA : the reduction of the population density of the excited state and the additional propagation losses. On Fig. 6(a), we plot the evolution of the excited population density  $n_2$  versus the pump power. It shows that ESA is responsible for a small variation of the population. As the output power  $P_{2D}$  for the LED-LC operating at full aperture ( $r=1$ ) is proportional to  $n_2$  (see Eq. (4)), this small variation does not affect the output power significantly. On the contrary, Fig. 6(b) shows a strong contribution of ESA to the loss coefficient, tripling the value at maximum pump power. This effect is mainly responsible for the 14% power drop on Fig. 2(b) for  $r=1$ .

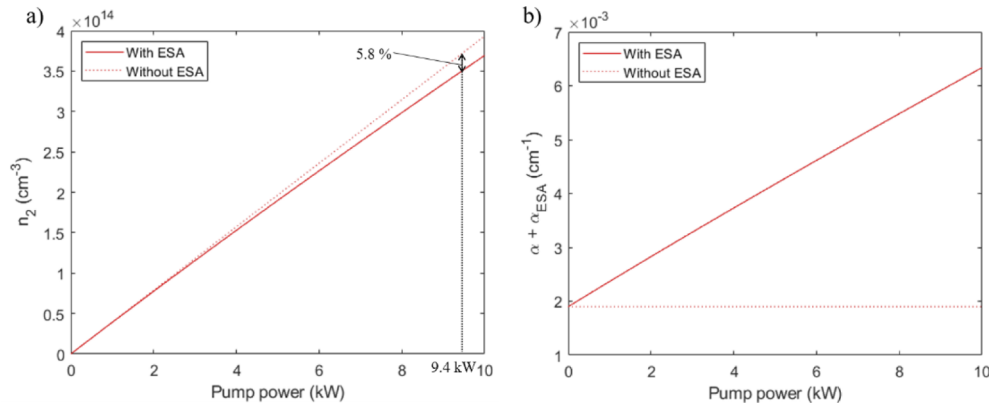


**Fig. 6.** Evolution of the population density of the excited state level (a) and the ESA loss coefficient (b) with the pump power.

### 3.3. Output power for a 3D-luminescent concentrator ( $r > 1$ )

In this section, light recycling occurs in the three dimensions of space, thanks to the back and the front mirrors. The output surface is reduced following the position of the front mirror, and its area is noted  $s$  ( $r = wt/s$ ). We assume that the light recycled inside the LC by the mirrors has a negligible impact on  $I_e$  because it undergoes much less reflections than the trapped light. Hence, it is assumed that the value of  $n_2$  depends only on the pump power and remains constant with  $r$ . Based on [15] and considering ESA, the power emitted by the output surface of the LC is:

$$P_{3D} = An_2wtl \frac{1}{r} \frac{hc (\cos \theta_{TIR} - 1)}{\lambda_e 2d_l(\alpha + \alpha_{ESA})} \frac{T_{Fresnel}(e^{-d_l(\alpha + \alpha_{ESA})} - 1)(1 + RT_{OA}^2 e^{-d_l(\alpha + \alpha_{ESA})})}{1 - e^{-2d_l(\alpha + \alpha_{ESA})} T_{OA}^2 \left[ R(1 - T_{Fresnel})\frac{1}{r} + \left(1 - \frac{1}{r}\right) R^2 \right]} \quad (6)$$

Equation (6) is used to plot the analytical curves on Fig. 2 and fits the experimental observations. It shows that ESA strongly reduces the output power, up to a factor 3 depending on the value of  $r$ . To understand this effect, we consider the average distance travelled by rays before finding the output. By using the sum of the terms of a geometric series and its first derivative, it can be shown that this distance is:  $(2r-1)d_l$  (see Supplement 1). Considering the losses mainly from the propagation losses (excluding other losses on mirrors or on interfaces), we can write the

transmission after the average travelled distance:

$$T_{av}(r) = e^{-(\alpha + \alpha_{ESA})(2r-1)d_l} \quad (7)$$

Figure 7 shows  $T_{av}(r)$  for two values of pump power. It shows that this transmission is strongly dependent on the pump power and on the value of  $r$ . This illustrates and explains why  $P_{3D}$  is much more sensitive to the effect of ESA when  $r$  increases (Fig. 2(b)).

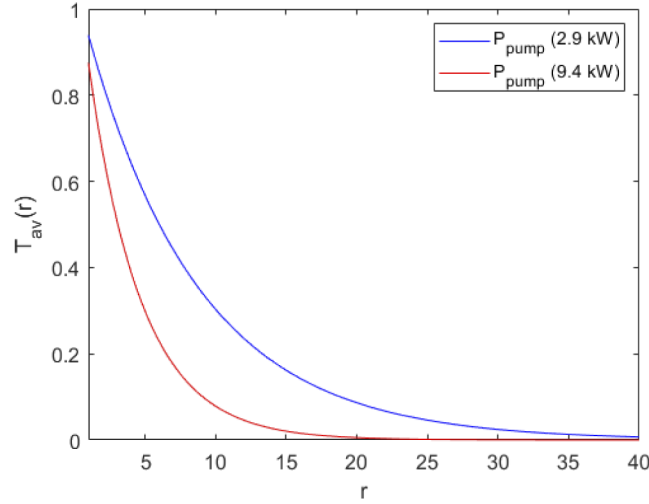


**Fig. 7.** Evolution of the transmission of the additional recycled light with  $r$  for the higher and lower pump powers.

#### 3.4. Brightness enhancement of the light recycling process at high pump power

The brightness enhancement ( $B_{3D}/B_{2D}$ ) by light recycling is described in [15]. The behavior of  $B_{3D}/B_{2D}$  corresponds to the sum of the terms of a geometric series as a small amount of light is emitted by the aperture after each roundtrip inside the luminescent concentrator. The equation in [15] is adapted to the presence of ESA in Eq. (8):

$$\frac{B_{3D}}{B_{2D}} = \frac{1 - e^{-2d_l(\alpha + \alpha_{ESA})} R T_{OA}^2 (1 - T_{Fresnel})}{1 - e^{-2d_l(\alpha + \alpha_{ESA})} T_{OA}^2 \left[ \frac{1 - T_{Fresnel}}{r} R + \left(1 - \frac{1}{r}\right) R^2 \right]} \quad (8)$$

Figure 8 gathers the brightness enhancement of the LC by light recycling. The dotted lines correspond to the analytical model in Eq. (8). The fit between the measured data and the analytical model fluctuates as it depends greatly on the uncertainty of the measurement of  $r$  and the uncertainty on the calculated emitted power density  $I_e$ . Despite this uncertainty, the right order of magnitude is reached for the brightness enhancement: a factor 5.1 for a LED pump power of 2.9 kW and a factor 3.2 for a LED pump power of 9.4 kW. The brightness enhancement tends to decrease when the pump power gets higher: this is due to the higher impact of ESA at higher pump powers.

Here, the brightness enhancements are lower than in [15] performed at low pump power level (best value of 13.5). This difference is explained by three main elements. Firstly, the length of the LC is 200 mm instead of 100 mm, this parameter has a great impact on the travelled distance and thus on the losses. Secondly, the presence of optical adhesive contacting the two Ce:YAG together, induces additional losses (Table 1). Finally, the presence of ESA generates additional losses at high pump power levels.

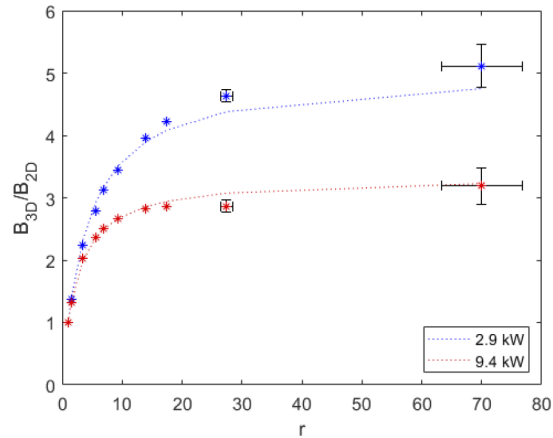


**Fig. 8.** Measured brightness enhancement of LC versus  $r$  for several LED pump power. The dotted lines correspond to Equ.8.

Including these 3 parameters in our model allows to retrieve the brightness enhancement factors correctly (Fig. 8). It is then obvious that high brightness and high power luminescent concentrators using Ce:YAG are challenging and require to take into account limiting phenomenon such as ESA that was up to now neglected. Compared to previous studies on Ce:YAG limitations using laser diode-pumped Ce:YAG “phosphor” [8], this result could be surprising at a first glance since the average pump intensity with LED is only  $1.8 \text{ W/mm}^2$  on the Ce:YAG faces, hundred times lower than the pump intensity of blue laser diodes. Likewise, the doping concentration is only of 0.11% in our case, 10 times lower than Ce:YAG phosphors. However, the main difference between a Ce:YAG phosphor and a Ce:YAG concentrator is the propagation length inside the medium : less than 1 mm in phosphor and higher than 1 m in a concentrator. This makes the concentrator very sensitive to loss variation hence to ESA.

#### 4. Conclusion

We demonstrated a 3D Ce:YAG luminescent concentrator pumped by 2 arrays of blue LEDs in quasi-continuous wave operation. Contrary to other 2D LED-LC, this 3D LED-LC can provide a small and squared output surface making the beam shaping easier for applications. For a  $1 \text{ mm}^2$  output surface, corresponding to a standard LED surface, the source emits a power of 145 W with a brightness of  $4.6 \text{ kW/cm}^2/\text{sr}$ , exceeding LED performance by a factor 35. By taking the spectral shape in account, this visible 3D LED-LC emit a luminous flux of  $7.6 \cdot 10^4 \text{ lm}$  and a brightness of  $2.4 \cdot 10^4 \text{ cd/mm}^2$  overcoming other visible sources like arc lamp, laser activated remote phosphor, and 2D luminescent concentrators typically by one order of magnitude and standing among the brightest incoherent light source ever build. Relying on the stability, ruggedness and lifetime of the LED technology, this source has the potential to become a reference for a large panel of applications.

This work gives a deep understanding of the performance limitation of LED-LC versus the pump power. The pump power increases the population density of the excited state and then increases the losses induced by excited state absorption. By this effect, the loss coefficient is tripled at maximum pump power. The analytical model estimating the output power in the presence of ESA is close to the experimental observations validating the role of ESA in LED-LC performance.

We believe that this work gives major keys to pave the way for new broadband sources combining power and exceptionally high brightness.

**Funding.** Centre National de la Recherche Scientifique (CNRS pre-maturation LEDsGO project); Agence Nationale de la Recherche (ANR-10-LABX-0039-PALM).

**Disclosures.** The authors declare no conflicts of interest.

**Data Availability.** Data underlying the results presented in this paper are not publicly available at this time but may be obtained from the authors upon reasonable request.

**Supplemental document.** See [Supplement 1](#) for supporting content.

## References

1. S. Nakamura, T. Mukai, and M. Senoh, "Candela-class high-brightness InGaN/AlGaIn double-heterostructure blue-light-emitting diodes," *Appl. Phys. Lett.* **64**(13), 1687–1689 (1994).
2. T. Mukai, M. Yamada, and S. Nakamura, "Characteristics of InGaIn-based UV/blue/green/Amber/red light-emitting diodes," *Jpn. J. Appl. Phys.* **38**, 3976–3981 (1999).
3. J. J. Wierer, J. Y. Tsao, and D. S. Sizov, "Comparison between blue lasers and light-emitting diodes for future solid-state lighting," *Laser Photonics Rev.* **7**(6), 963–993 (2013).
4. R. W. Boyd, "Radiometry and the Detection of Optical Radiation," Wiley (1983).
5. Y. Shimizu, K. Sakano, Y. Noguchi, and T. Moriguchi, Japanese priority patent applications to U. S. Patent 5, 925 (1996).
6. P. Schlotter, R. Schmidt, and J. Schneider, "Luminescence conversion of blue light emitting diodes," *Appl. Phys. A* **64**(4), 417–418 (1997).
7. S. Arjoca, E. G. Villora, D. Inomata, K. Aoki, Y. Sugahara, and K. Shimamura, "Temperature dependence of Ce:YAG sing-crystal phosphors for high-brightness white LEDs/LDs," *Mater. Res. Express* **2**(5), 055503 (2015).
8. A. Lenef, M. Raukas, J. Wang, and C. Li, "Phosphor performance under high intensity excitation by InGaIn laser diodes," *ECS J. Solid State Sci. Technol.* **9**(1), 016019 (2020).
9. Y. Yang, S. Zhuang, and B. Kai, "High brightness laser-driven white emitter for Etendue-limited applications," *Appl. Opt.* **56**(30), 8321 (2017).
10. S. Li, L. Wang, N. Hirotsaki, and R. Xie, "Color conversion materials for high-brightness laser driven solid-state lighting," *Laser Photonics Rev.* **12**(12), 1800173 (2018).
11. Mehran Rafiee, Subhash Chandra, Hind Ahmed, and Sarah J. McCormack, "An overview of various configurations of Luminescent Solar Concentrators for photovoltaic applications," *Opt. Mater.* **91**, 212–227 (2019).
12. P. Pichon, A. Barbet, J.-P. Blanchot, F. Druon, F. Balembois, and P. Georges, "Light-emitting diodes, a new paradigm for Ti:sapphire pumping," *Optica* **5**(10), 1236–1239 (2018).
13. J. Sathian, J. D. Breeze, B. Richards, N. M. Alford, and M. Oxborrow, "Solid-state source of intense yellow light based on a Ce:YAG luminescent concentrator," *Opt. Express* **25**(12), 13714–13727 (2017).
14. D. K. G. de Boer, D. Bruls, and H. Jagt, "High-brightness source based on luminescent concentration," *Opt. Express* **24**(14), A1069–1074 (2016).
15. A. Barbet, A. Paul, T. Gallinelli, F. Balembois, J.-P. Blanchot, S. Forget, S. Chénais, F. Druon, and P. Georges, "Light-emitting diode pumped luminescent concentrators : a new opportunity for low-cost solid-state lasers," *Optica* **3**(5), 465–468 (2016).
16. P. Pichon, A. Barbet, D. Blengino, P. Legavre, T. Gallinelli, F. Druon, J.-P. Blanchot, F. Balembois, S. Forget, S. Chénais, and P. Georges, "High-radiance light sources with LED-pumped luminescent concentrators applied to pump Nd:YAG passively Q-switched laser," *Opt. Laser Technol.* **96**, 7–12 (2017).
17. P. Pichon, F. Balembois, F. Druon, and P. Georges, "3D luminescent concentrators," *Opt. Express* **29**(5), 6915 (2021).
18. M. J. Weber, "Nonradiative decay from 5d-states of rare earth in crystals," *Solid State Commun.* **12**(7), 741–744 (1973).
19. D. S. Hamilton, S. K. Gayen, G. J. Pogatsnik, and D. Ghen, "Optical-absorption and photoionization measurements from the excited states of  $\text{Ce}^{3+}:\text{Y}_3\text{Al}_5\text{O}_{12}$ ," *Phys. Rev. B* **39**(13), 8807–8815 (1989).
20. R. R. Jacobs, W. F. Krupke, and M. J. Weber, "Measurement of excited-state-absorption loss for  $\text{Ce}^{3+}$  in  $\text{Y}_3\text{Al}_5\text{O}_{12}$  and implications for tunable 5d-4f rare-earth lasers," *Appl. Phys. Lett.* **33**(5), 410–412 (1978).
21. W. J. Miniscalco, J. M. Pellegrino, and W. M. Yen, "Measurements of excited-state absorption in  $\text{Ce}^{3+}:\text{YAG}$ ," *J. Appl. Phys.* **49**(12), 6109–6111 (1978).